Influence of background heterogeneity on traveltime shifts for compacting reservoirs

Rodrigo F. Fuck[1,2], Ilya Tsvankin[2]* and Andrey Bakulin[3]

[1]*Schlumberger Cambridge Research, High Cross, Madingley Road, Cambridge, CB3 0EL, UK,* [2]*Center for Wave Phenomena, Colorado School of Mines, Golden, CO 80401, USA, and* [3]*WesternGeco, 10001 Richmond Avenue, Houston, TX 77042-4299, USA*

ABSTRACT

Compaction induced by pore-pressure decrease inside a reservoir can be monitored by measuring traveltime shifts of reflection events on time-lapse seismic data. Recently we introduced a perturbation-based formalism to describe traveltime shifts caused by the 3D stress-induced velocity field around a compacting reservoir. Application of this method to homogeneous background models showed that the offset variation of traveltime shifts is controlled primarily by the anisotropic velocity perturbations and can provide valuable information about the shear and deviatoric stresses.

Here, we model and analyse traveltime shifts for compacting reservoirs whose elastic properties are different from those of the surrounding medium. For such models, the excess stress is influenced primarily by the contrast in the rigidity modulus μ across the reservoir boundaries. Synthetic examples demonstrate that a significant (25% or more) contrast in μ enhances the isotropic velocity perturbations outside the reservoir. Nevertheless, the influence of background heterogeneity is mostly confined to the reservoir and its immediate vicinity and the anisotropic velocity changes are still largely responsible for the offset dependence of traveltime shifts. If the reservoir is stiffer than the host rock, the background heterogeneity reduces anisotropic velocity perturbations inside the reservoir but increases them in the overburden. As a result, in this case, the magnitude of the offset variation of traveltime shifts is generally higher for reflections from interfaces above the reservoir.

We also study compaction-induced stress/strain and traveltime shifts for a stiff reservoir embedded in a softer layered model based on velocity profiles from the Valhall Field in the North Sea. Despite producing discontinuities in strain across medium interfaces, horizontal layering does not substantially alter the overall behaviour of traveltime shifts. The most pronounced offset variation of traveltime shifts is observed for overburden events recorded at common midpoints close to the reservoir edges. On the whole, prestack analysis of traveltime shifts should help better constrain compaction-induced velocity perturbations in the presence of realistic background heterogeneity.

Key words: Compacting reservoirs, Excess stress, Heterogeneous media, Time-lapse seismic, Traveltime shifts.

INTRODUCTION

Traveltime shifts (i.e., the differences in traveltime for the same reflector measured between time-lapse seismic surveys)

*E-mail: ilya@dix.mines.edu

have become a common tool for monitoring dynamic changes in hydrocarbon reservoirs caused by depletion. For example, Guilbot and Smith (2002) employed traveltime shifts to detect and monitor reservoir compaction and surface subsidence at the Ekofisk Field in the North Sea. Hatchell and Bourne (2005b) introduced a method to estimate the ratio of the perturbations in the vertical velocity and vertical strain from traveltime shifts measured on stacked data. This ratio (R) can be used to monitor compaction and detect compartments in a reservoir. Hodgson *et al.* (2007) computed the vertical derivatives of traveltime shifts on stacked data to estimate pressure changes in the Genesis reservoir.

In a recent paper (Fuck, Bakulin and Tsvankin 2009), we derived an analytic expression for traveltime shifts that provides valuable physical insight into the influence of compaction-related stress on reflection traveltimes. In contrast to previous work (e.g., Landrø and Stammeijer 2004; Hatchell and Bourne 2005a; Roste, Stovas and Landrø 2006), our solution describes traveltime shifts for arbitrary source-receiver offsets while honouring the fact that reservoir compaction produces heterogeneous, anisotropic velocity perturbations. The numerical examples in Fuck *et al.* (2009) are given for the simple model of a 2D homogeneous halfspace (i.e., the elastic properties throughout the pre-stressed halfspace are the same), with pore-pressure changes confined to a rectangular reservoir. When the background medium is homogeneous, traveltime shifts in this model are primarily controlled by the anisotropic velocity perturbations, which should be estimated from prestack data.

The goal of this paper is to analyse traveltime shifts for a compacting reservoir embedded in a heterogeneous pre-stressed (background) medium. We start by reviewing the approximation for traveltime shifts developed by Fuck *et al.* (2009) and the main properties of the excess stress and strain fields for homogeneous background models. Then we conduct geomechanical simulations of compaction-induced stress and compute traveltime shifts for a model containing a rectangular reservoir with the elastic parameters different from those of the host rock. Numerical testing indicates that traveltime shifts vary with the contrast in the rigidity modulus μ across the reservoir boundaries but are almost insensitive to the contrast in the P-wave velocity and density. Finally, we examine a more complicated, layered background model with the interval parameters adapted from depth profiles measured at the Valhall Field in the North Sea.

THEORETICAL BACKGROUND

Excess stress and strain for compacting reservoirs

Compaction of hydrocarbon reservoirs results from both elastic and anelastic deformation induced by depletion. In general, elastic deformation is caused by the pore-pressure drop inside the reservoir; anelastic (i.e., irreversible) deformation may include the crushing of grains and pores or dissolution of reservoir rocks by fluids injected to enhance oil recovery. Compaction may be largely controlled by poroelastic phenomena but anelastic deformation (e.g., related to water weakening) could be just as important in some chalk reservoirs, such as Ekofisk (Sylte *et al.* 1999).

We restrict our treatment to elastic strains, following the approach of Geertsma (1973), Segall (1992) and Segall, Grasso and Mossop (1994), who successfully explained depletion-induced phenomena using linear poroelastic behaviour of reservoir rocks. Poroelastic rocks can be deformed not only by external forces but also by pressure changes inside the pores (e.g., Wang 2000). Due to spatial variations of the pore-pressure changes in the reservoir, the excess stress/strain field includes not only normal but also shear components.

If the pre-stressed medium is homogeneous and the reservoir has a relatively simple shape, it is possible to obtain analytic solutions for the particle displacement, stress and strain. For instance, Hu (1989) presented a concise 3D description of the excess stress field for a reservoir that has the shape of a parallelepiped. Such analytic developments provide important physical insight into compaction-induced phenomena. In particular, if the pre-stressed medium is homogeneous, the volumetric strain changes (i.e., the trace Δe_{kk} of the strain tensor) vanish outside the reservoir (Hu 1989), while Δe_{kk} inside the reservoir is constant (Downes, Faux and O'Reilly 1997). Volumetric changes outside the reservoir occur only if the model includes a free surface. In that case, the largest values of Δe_{kk} outside the reservoir are observed near the surface (Hu 1989); the magnitude of this anomaly decreases for deeper reservoirs.

Furthermore, it can be inferred from the equations of Hu (1989) that the deviatoric stress changes $\Delta \sigma_{ij}$ are inversely proportional to the squared ratio of the P- and S-wave velocities (V_P/V_S):

$$\Delta \sigma_{ij} \propto \left(\frac{V_S}{V_P} \right)^2 \alpha \Delta P \,, \tag{1}$$

where ΔP is the pore-pressure change inside the reservoir and α is the Biot-Willis coefficient[1]. The deviatoric strain ($\Delta\epsilon_{ij} = \Delta e_{ij} - \frac{1}{3}\Delta e_{kk}$) and stress changes are related by Hooke's law for isotropic media:

$$\Delta\sigma_{ij} = 2\mu\Delta\epsilon_{ij}\,. \tag{2}$$

Substituting equation (2) into equation (1), we find

$$\Delta\epsilon_{ij} \propto \frac{\alpha\Delta P}{\rho V_P^2}\,; \tag{3}$$

ρ is the density. The volumetric strain change is given by

$$\Delta e_{kk} \propto \frac{\alpha\Delta P}{\rho V_P^2}\frac{g}{(3-4g)} \approx \frac{\alpha\Delta P}{\rho V_P^2}\frac{g}{3}\left(1+\frac{4g}{3}\right), \tag{4}$$

where $g = (V_P/V_S)^{-2}$. Since typically $g \ll 1$, Δe_{kk} is inversely proportional to both V_P^2 and V_P^2/V_S^2.

Traveltime shifts

To give an analytic description of P-wave traveltime shifts above a compacting reservoir, Fuck *et al.* (2009) assumed the compaction-induced velocity changes to be small. Traveltime shifts are then obtained from the first-order perturbation of traveltimes along reference rays traced in the background model. The approximation of Fuck *et al.* (2009) includes two terms, one of which is 'geometric' (i.e., the time shift related to the displacement of the sources, receivers and interfaces), while the other depends on the velocity perturbations along the ray. Since the compaction-related displacements in the elastic regime are on the order of centimetres, they yield relatively small traveltime shifts. Hence, the geometric term can be neglected. To satisfy the assumption of elastic deformation, the methodology proposed by Fuck *et al.* (2009) should be applied to time-lapse surveys acquired less than two years or so apart.

Using the non-linear theory of elasticity, the stiffness tensor c_{ijkl} of the deformed medium can be represented as

$$c_{ijkl} = c_{ijkl}^{\circ} + c_{ijklmn}\Delta e_{mn}\,, \tag{5}$$

where c_{ijkl}° is the stiffness tensor of the background medium, c_{ijklmn} is the strain-sensitivity tensor and Δe_{mn} is the tensor of the elastic strains induced by the reservoir compaction. Hereafter, the summation convention over repeated indices is assumed.

It is convenient to rewrite equation (5) by employing Voigt notation, which maps each pair of indices *ij* to a single

index ν

$$\nu = i\delta_{ij} + (9-i-j)(1-\delta_{ij})\,, \tag{6}$$

where δ_{ij} is Kronecker's symbol. The strain tensor Δe_{mn} then becomes a vector (denoted by ΔE_γ) and equation (5) takes a concise matrix form (Fuck and Tsvankin 2009):

$$C_{\nu\beta} = C_{\nu\beta}^{\circ} + C_{\nu\beta\gamma}\Delta E_\gamma\,. \tag{7}$$

A detailed analysis of the symmetry of the deformed medium based on equation (5) can be found in Fuck and Tsvankin (2009).

Assuming both the background stiffness tensor and the strain-sensitivity tensor to be isotropic, the velocity-related P-wave traveltime shifts are obtained as (Fuck *et al.* 2009):

$$\delta t = -\frac{1}{2}\int_{\tau_1}^{\tau_2}\Big[\underbrace{B_1\Delta e_{kk}}_{\text{volumetric}} + \underbrace{B_2(\mathbf{n}^{\mathrm{T}}\Delta\epsilon\,\mathbf{n})}_{\text{deviatoric}}\Big]\mathrm{d}\tau\,, \tag{8}$$

where $\mathbf{n}$ is the unit slowness vector of the reference ray and τ is the time along the ray. The constants B_1 and B_2 are given by

$$B_1 = \frac{C_{111} + 2C_{112}}{3C_{33}^{\circ}}\,, \tag{9}$$

$$B_2 = \frac{4C_{155}}{C_{33}^{\circ}}\,. \tag{10}$$

Since $C_{155} = (C_{111} - C_{112})/4$, traveltime shifts in equation (8) depend on just two combinations of the three linearly independent elements $C_{\nu\beta\gamma}$ of the isotropic tensor c_{ijklmn}. Equation (8) separates the velocity-related traveltime shifts into the isotropic term, which depends on the volumetric strain (Δe_{kk}) and the anisotropic term associated with the deviatoric strain elements ($\Delta\epsilon_{ij}$). Note that instead of using the deviatoric stress (as Fuck *et al.* 2009) in equation (8), we express the traveltime shifts in terms of the deviatoric strain. This is done to facilitate comparison between the contributions of the isotropic and anisotropic velocity changes.

MODELLING METHODOLOGY

Following Fuck *et al.* (2009), we employ a three-step procedure to simulate depletion-related traveltime shifts. First, the excess stress and strain fields are computed for 2D models with a heterogeneous background. The exact meaning of 'background heterogeneity' is explained below. We use the finite-element method (COMSOL™ package) to solve for the displacements, stresses and strains caused by a pore-pressure drop inside a rectangular reservoir. This methodology is

---

[1] α varies from 0 to 1 and quantifies the pore-pressure response to external forces.

based on a plane-strain model, with no deformation in the x_2-direction. The top of the model is specified as a free surface; to avoid artefacts due to the finite model dimensions, the model's height and width are 10 times larger than those of the reservoir.

At the second step, we compute the stiffness and velocity perturbations from the strain changes using equation (7). Finally, the traveltime shifts are obtained either from approximation (8) or by subtraction of the exact (ray-traced) traveltimes calculated for the perturbed and background velocity models. The anisotropic ray-tracing algorithm is based on the equations of Červený (2001) for heterogeneous anisotropic media, which are solved by the fifth-order Runge-Kutta method (Press *et al.* 1992). To avoid errors in traveltime shifts caused by smoothing of velocity models, we account for reflection/transmission at interfaces using Snell's law.

NUMERICAL RESULTS

This section is divided into two parts. First, we analyse models in which the reservoir is embedded in an otherwise homogeneous half-space ('homogeneous host rock' models). Second, we present the results for a more realistic layered model based on velocity profiles from the Valhall Field in the North Sea.

Homogeneous host rock models

We introduce a contrast in the P- or S-wave velocity between the undeformed reservoir and the host rock, while the density and the strain-sensitivity matrix $C_{\upsilon\beta\gamma}$ are kept constant (Fig. 1). The velocity contrast before the pore-pressure drop inside the reservoir ranges from 0–50%; the reference values for the stiffness constants and the strain-sensitivity tensor are taken from published laboratory data for Berea sandstone (Sarkar, Bakulin and Kranz 2003). For all numerical experiments, the pore-pressure drop is fixed at $\Delta p = -5$ MPa.

To simulate the static stiffnesses, which are generally smaller than those computed from traveltimes (Yale and Jamieson 1994), the velocities were multiplied by 0.9. The same scaling coefficient was used in the tests of Fuck *et al.* (2009).

Stress/strain modelling

The most prominent change caused by the velocity contrast across the reservoir boundary is the presence of a non-zero volumetric strain Δe_{kk} outside the reservoir that is not related to surface subsidence (Fig. 2). This Δe_{kk} anomaly, however,
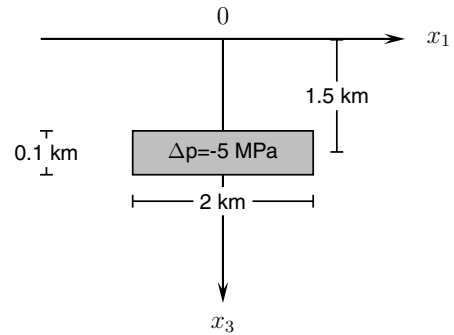

Figure 1. 2D model of a rectangular reservoir embedded in an isotropic homogeneous medium. The pressure drop inside the reservoir is 5 MPa. The medium parameters are taken from the laboratory data of Sarkar *et al.* (2003) for Berea sandstone: $V_P = 2.3$ km/s, $V_P/V_S = 1.58$, $\rho = 2.14$ g/cm^3, $C_{111} = -13904$ GPa, $C_{112} = 533$ GPa and $C_{155} = -3609$ GPa. To compute the excess stress, the Biot-Willis coefficient α was set to 0.85 (the closer α is to unity, the more stress is generated by reducing the pore pressure inside the reservoir).
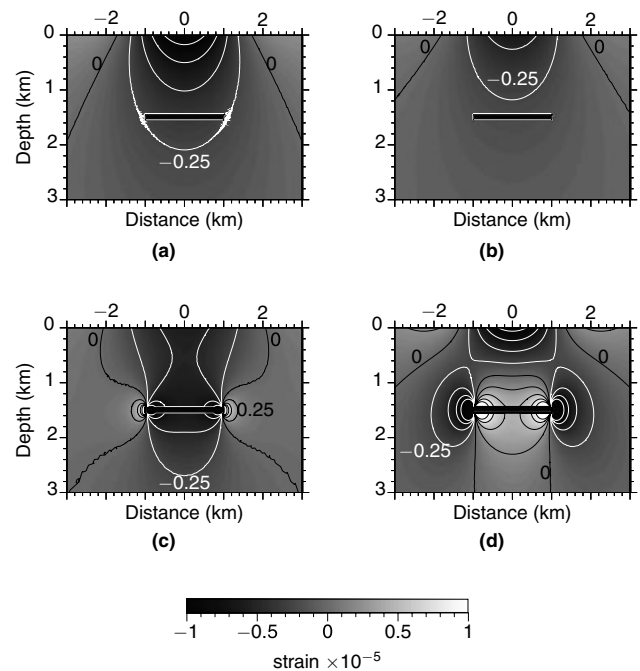

Figure 2. Compaction-related volumetric strain Δe_{kk} for models with different elastic contrast between the reservoir and host rock. a) No elastic contrast across the reservoir boundaries; b) the velocity V_P is 25% higher outside the reservoir; c) the velocity V_S is 20% lower outside the reservoir; d) V_S is 20% higher outside the reservoir. Negative values are contoured in white, zero and positive values in black. The contour step is 0.25×10^{-5}.
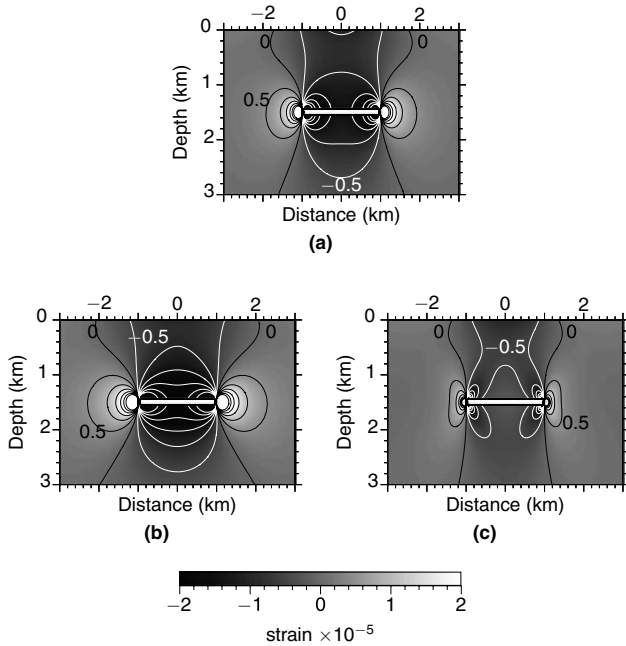
(a)

(b)

(c)

strain $\times 10^{-5}$

Figure 3. Influence of the contrast in the rigidity modulus μ on the compaction-related horizontal deviatoric strain Δe_{11}. a) No elastic contrast across the reservoir boundaries; b) the velocity V_S is 20% lower outside the reservoir; c) V_S is 20% higher outside the reservoir. The contrast in V_S is equivalent to the contrast in μ because the density is held constant. The contour step is 0.5×10^{-5}.

is observed only when there is a contrast in the rigidity modulus μ, which is in agreement with the semi-analytic results of Soltanzadeh, Hawkes and Sharma (2007). Indeed, for models with no contrast in μ the pattern of the subsurface distribution of Δe_{kk} is similar to that for a homogeneous background model (Fig. 2b). In contrast, Fig. 2(c,d) shows completely different patterns of the subsurface volumetric changes caused by the contrast in μ. The spatial distribution of Δe_{kk} also depends on whether the reservoir is more or less rigid than the host rock (compare Figs 2c and 2d).

The deviatoric strain distribution around the reservoir is also sensitive to the contrast in the rigidity modulus (Fig. 3). In particular, if the reservoir rocks are relatively stiff, the deviatoric strain increases toward the reservoir and concentrates near its boundaries. For a softer reservoir, the deviatoric strain spreads throughout the section (especially in the vertical direction) and tends to accumulate at the reservoir corners[2].

Figure 4 illustrates how the volumetric and deviatoric ($\Delta \varepsilon_{ij} = \Delta \sigma_{ij} / 2\mu$) strains at the centre of the reservoir depend

---

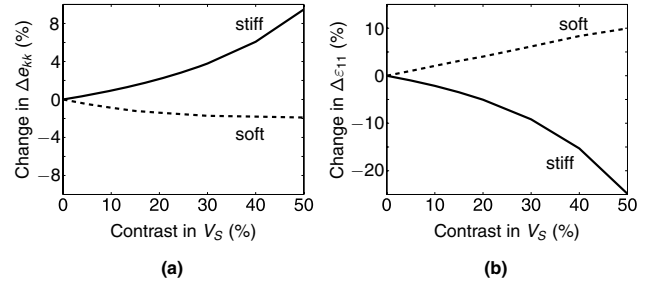[2] The deviatoric vertical and shear strains exhibit patterns similar to that for the horizontal strain component in Fig. 3.

(a)

(b)

Figure 4. Compaction-related strain at the centre of the reservoir (0 km, 1.5 km) as a function of the contrast in V_S (i.e., in μ). The strain for the homogeneous background model is subtracted from that for models with a variable contrast in V_S. a) The volumetric strain; b) the deviatoric horizontal strain.

on the contrast in V_S (note that the density is constant) across its boundaries. A stiffer reservoir produces larger volumetric and smaller deviatoric strains compared with the homogeneous background model, which increases the contribution of the isotropic velocity changes for reflectors at the base of the reservoir and beneath it. For softer reservoirs, the opposite is true (Fig. 4). Exceptions include uncommon reservoirs that have an anomalously high or low P-wave velocity and low ratio V_P/V_S. For such models, however, the changes in the volumetric and deviatoric strains caused by the background heterogeneity are comparable. Hence, the relative contributions of the isotropic and anisotropic velocity perturbations to the traveltime shifts remain almost the same.

Finally, note that the patterns observed in Figs 2 and 4a) confirm that equation (4), derived for a homogeneous background, remains qualitatively valid for the more complicated model treated here.

Offset variation of traveltime shifts

Two important issues discussed here are the magnitude of the variation of traveltime shifts with offset and the influence of the anisotropic velocity perturbations on this variation. Even if the offset variation is detectable, it provides new information about the excess stress field only if traveltime shifts are dominated by the anisotropic velocity changes. Otherwise, compaction-related velocity perturbations can be estimated from traveltime shifts on stacked data.

For homogeneous background models, the offset variation of traveltime shifts is significant, especially for reflectors below the reservoir. Despite the large magnitude of the isotropic velocity changes inside the reservoir, this offset dependence (even
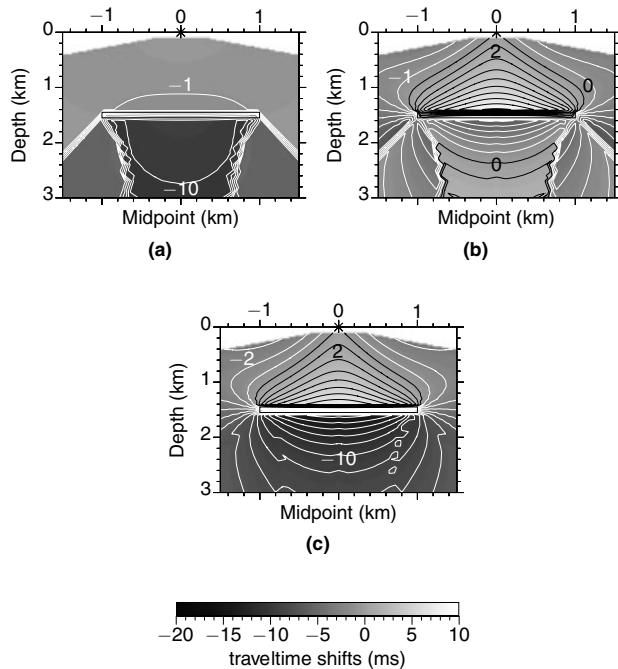
Figure 5. Approximate traveltime shifts (computed from equation (8)) for a shot above the centre of the reservoir. The shift plotted at each (x, z) point corresponds to the reflection from an imaginary horizontal interface at depth z recorded at the source-receiver offset $2x$. The background velocity V_S is 20% smaller outside the reservoir. The traveltime shifts caused by the a) isotropic and b) anisotropic velocity changes; c) the total shifts.
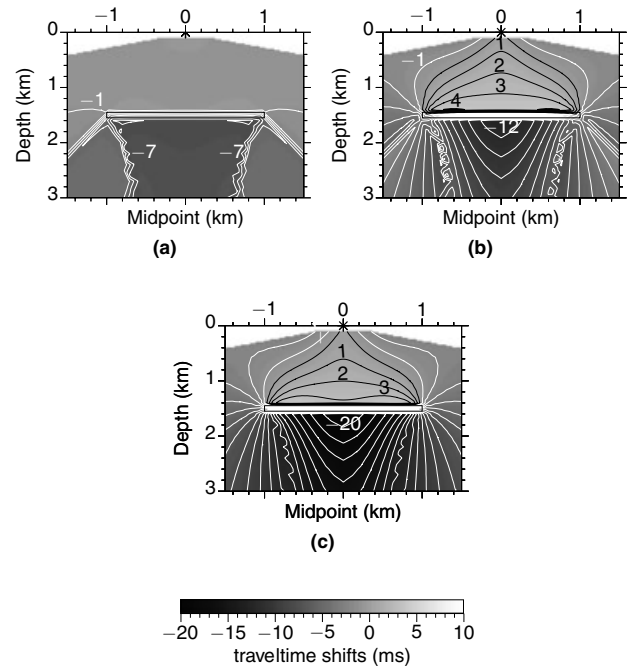
Figure 6. Approximate traveltime shifts for a shot above the center of the reservoir. The background velocity V_S is 20% larger outside the reservoir. The traveltime shifts caused by the (a) isotropic and (b) anisotropic velocity changes; (c) the total shifts.

for deep events) is controlled primarily by the anisotropic velocity perturbations (Fuck *et al.* 2009).

As expected from the above results of stress and strain modeling, the behaviour of traveltime shifts in the absence of the contrast in μ is similar to that for a homogeneous background. Hence, anisotropic velocity perturbations are largely responsible for traveltime shifts generated in the overburden, as well as for the offset variation of traveltime shifts below the reservoir.

A contrast in μ across the reservoir boundaries, however, can cause significant changes in the behavior of traveltime shifts. As illustrated by Fig. 5, both the magnitude and offset variation of the traveltime shifts increase for reflections from interfaces above a more rigid reservoir. Conversely, when the reservoir is softer than the host rock, the magnitude of traveltime shifts and their offset variation increase for reflectors beneath the reservoir (Fig. 6).

These changes in the properties of the traveltime shifts can be explained by the influence of the contrast in μ on the compaction-induced strain. For example, traveltime shifts above the reservoir are caused mostly by the deviatoric strains.

Therefore, the larger deviatoric strains observed above a more rigid reservoir (compare Figs 3b and 3c) produce larger traveltime shifts with more pronounced offset variation. Traveltime shifts beneath the reservoir are strongly dependent on the strains accumulated inside it. In particular, the reduction in the volumetric strain and increase in the deviatoric strains inside a softer reservoir (Fig. 4a,b) result in a more pronounced offset variation of traveltime shifts for deep reflectors.

Figure 7 illustrates how the contrast in μ influences the behaviour and composition of traveltime shifts. In general, traveltime shifts vary more rapidly with offset, if the contrast in μ increases the deviatoric strains above the reflector. On the whole, offset-dependent traveltime shifts for this group of models are governed primarily by the anisotropic velocity perturbations.

Layered model

Next, we examine a model that consists of eight horizontal layers whose parameters are adapted from velocity profiles estimated at the Valhall Field in the North Sea (Fig. 8). The components of the strain-sensitivity tensor are taken from the measurements for North Sea shales made by Prioul, Bakulin
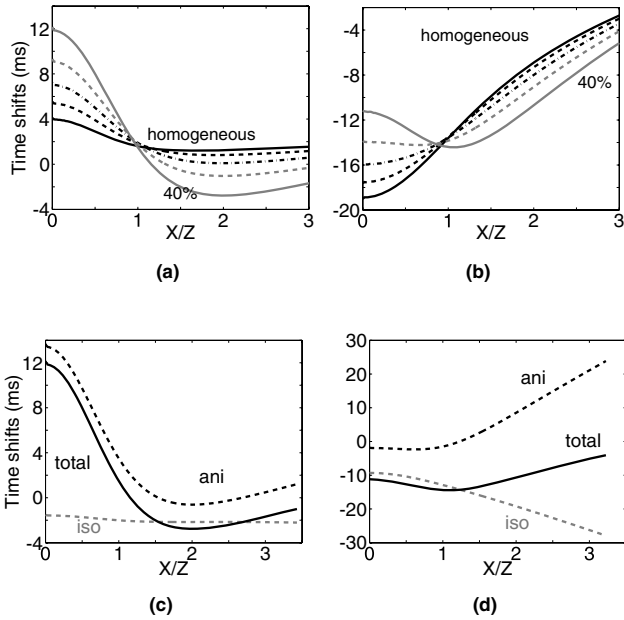
Figure 7. Influence of the contrast in V_S for a relatively stiff reservoir on traveltime shifts in common-midpoint (CMP) geometry; the CMP is located above the centre of the reservoir. The shifts are computed for the a) top and b) bottom of the reservoir; the contrast in V_S varies from 0% (solid black line) to 40% (solid grey) in steps of 10%; X/Z is the offset-to-depth ratio. The decomposition of the traveltime shifts for the c) top and d) bottom of the reservoir into the isotropic (iso) and anisotropic (ani) components; the contrast in V_S is 40%.
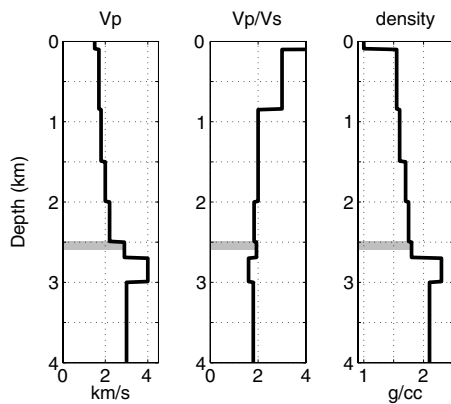

Figure 8. Velocity and density profiles adapted from published results for the Valhall Field in the North Sea. The model is composed of eight homogeneous layers and the rectangular reservoir (grey bar) is located inside layer 6. The first layer (water) is 100 m thick, with $C_{\upsilon\beta\gamma} = V_S = 0$. For layers two through four, $C_{111} = -11300$ GPa, $C_{112} = -4800$ GPa and $C_{123} = 5800$ GPa. For layers five through eight, $C_{111} = -3100$ GPa, $C_{112} = -800$ GPa and $C_{123} = 40$ GPa.

and Bakulin (2004) under two different ranges of hydrostatic load. Taking into account the weight of the overburden, the layers above 2 km were assigned the values of $C_{\upsilon\beta\gamma}$ for the load ranging from 5–30 MPa (except for the water (0–0.1 km) where $C_{\upsilon\beta\gamma} = 0$); the deeper layers were assigned $C_{\upsilon\beta\gamma}$ measured for the load between 30–100 MPa. To obtain the static velocity values similar to those published by Herwanger and Horne (2005, 2009) for their Valhall model, the seismic velocities were reduced by 40%.

Stress/strain modelling

Apart from the discontinuities in strain across the layer boundaries, the compaction-induced strains for the layered model are generally similar to those observed for the simpler models investigated in the previous section. For example, since the reservoir is stiffer than the overburden rocks, the deviatoric strains tend to concentrate around the reservoir rather than spread through the upper part of the model (Fig. 9). Also, as predicted by equation (3), the deviatoric strains are smaller beneath the reservoir than above it because of the higher P-wave velocities in the two bottom layers (Fig. 9a–c).

The volumetric strain Δe_{kk} is largely confined to the reservoir, where it exceeds the deviatoric strain $\Delta\epsilon_{ij}$. Outside the reservoir, however, the deviatoric strains dominate the strain field (compare Figs 9a and 9d). Some of the features of the distribution of the volumetric strain can be explained using equation (4). For instance, because Δe_{kk} is inversely proportional to V_P^2/V_S^2, the largest volumetric strain outside the reservoir is accumulated in the seventh layer, which has a small value of $V_P/V_S = 1.6$.

Figure 10 summarizes the influence of the compaction-induced strains on the velocity perturbations. As expected from our previous results (Fuck *et al.* 2009), the initially isotropic velocity model composed of homogeneous layers becomes anisotropic with a heterogeneous velocity field inside each layer. For our 2D model, the anisotropy in all layers is elliptical with a tilted symmetry axis (in 3D the symmetry becomes orthorhombic). Because the strain-sensitivity elements $C_{\upsilon\beta\gamma}$ are much larger for the shallow layers (down to 2 km), the velocity perturbations are restricted primarily to the upper part of the model (Fig. 10a). According to the sign of the Thomsen anisotropy parameter $\varepsilon = \delta$, the horizontal velocity is higher than the vertical velocity outside the reservoir ($\varepsilon > 0$) and smaller inside it ($\varepsilon < 0$, Fig. 10a). The rotation of the symmetry axis from the vertical (caused by the shear strain) does not exceed 1°.
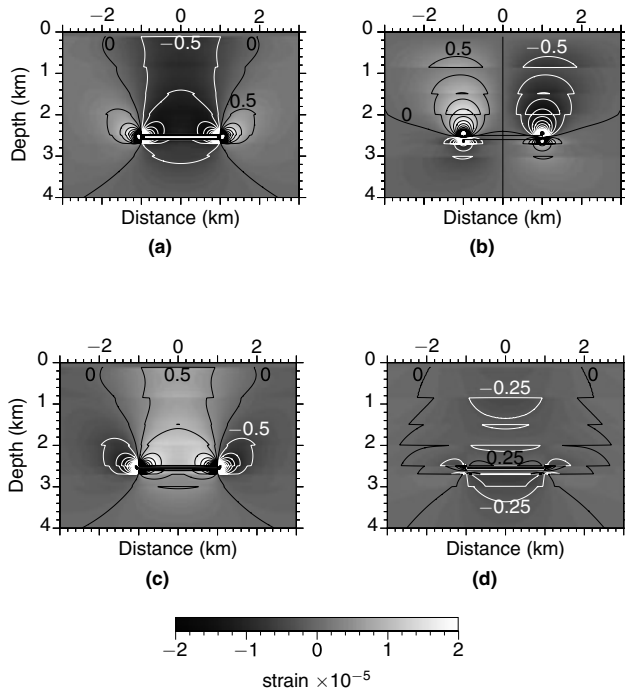
Figure 9. Deviatoric and volumetric strains caused by the pore-pressure drop $\Delta p = -2.5$ MPa inside the reservoir for the model from Fig. 8. The deviatoric strains (a) $\Delta\epsilon_{11}$, (b) $\Delta\epsilon_{13}$, (c) $\Delta\epsilon_{33}$ and (d) the volumetric strain Δe_{kk}. Negative strain values are contoured in white, positive values in black. The contour step is 0.5×10^{-5} in (a), (b), and (c), and 0.25×10^{-5} in (d). The colour scale is clipped for better contrast. At the centre of the reservoir (0 km, 2.55 km), $\Delta\epsilon_{11} = 1.2 \times 10^{-4}$, $\Delta\epsilon_{33} = -2.5 \times 10^{-4}$ and $\Delta e_{kk} = -3.9 \times 10^{-4}$.

Offset variation of traveltime shifts

Figure 11 displays ray-traced and approximate traveltime shifts for a common midpoint (CMP) located above the reservoir centre and a range of reflector depths. In contrast to the results of Fuck *et al.* (2009) for the homogeneous model, approximation (8) is more accurate for deeper reflectors because the largest velocity perturbations are concentrated in the upper part of the section.

Another factor contributing to the poor performance of the linearized approximation for reflectors at the shallow depths (0.85 km, 1.5 km and 2 km) is significant ray bending, which is not taken into account by equation (8). Ray bending makes the traveltimes more sensitive to the horizontal and shear components of the deviatoric strain tensor, which increases the offset variation of the exact (ray-traced) shifts. Also, the approximation deteriorates for common midpoints near the edges of the reservoir due to the pronounced accumulation of the shear strain around the reservoir corners (see Fig. 9b). In particular,
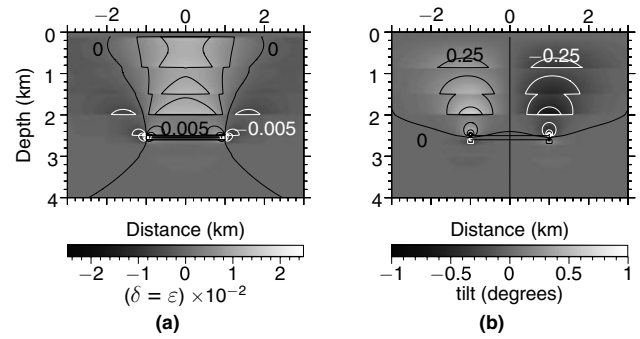

Figure 10. Stress-induced velocity anisotropy for the model in Fig. 8. a) The Thomsen parameter $\delta = \varepsilon$ and b) the tilt of the symmetry axis from the vertical. Positive values on both plots are contoured in black, negative values in white. Positive tilt implies clockwise axis rotation from the vertical.
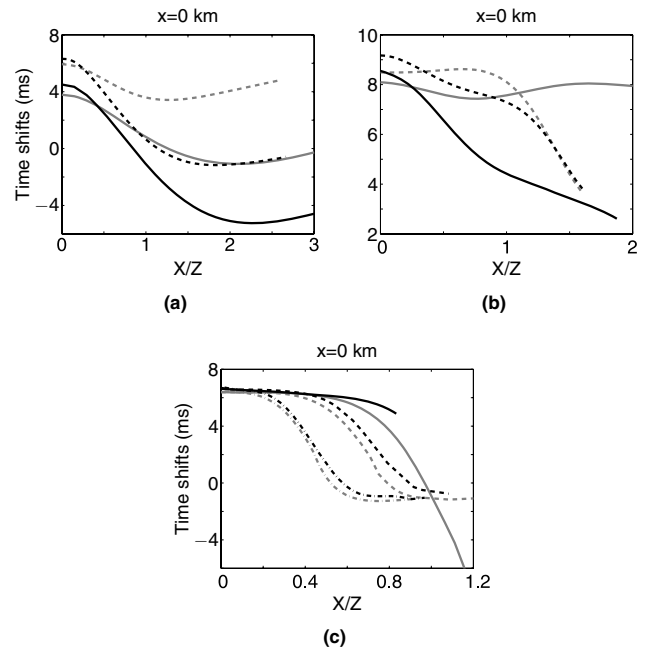

Figure 11. Comparison between ray-traced (black lines) and approximate (grey) traveltime shifts for a CMP above the reservoir centre. The shifts are computed for the reflectors at a) 0.85 km (solid lines) and 1.5 km (dashed), b) 2 km (solid) and 2.5 km (dashed) and c) 2.7 km (solid), 3 km (dashed) and 4 km (dash-dotted).

the difference between the ray-traced and approximate traveltime shifts for reflectors above the reservoir increases as the CMP approaches the reservoir edge located at $x = 1$ km.

Since the compaction-induced velocity perturbations occur mostly above the reservoir, the largest shifts (as well as their most pronounced offset variation) are observed for the overburden events, especially in common midpoints located above the reservoir corners (Fig. 12). As was the case for the
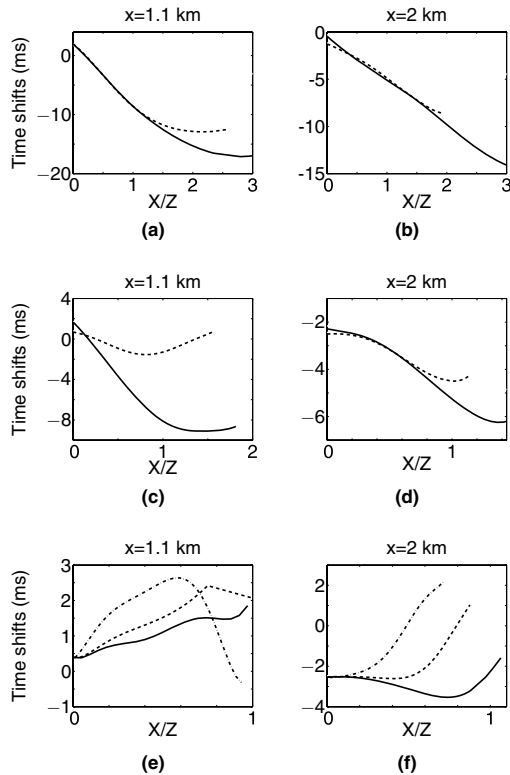
(a)   **(b)**

(c)

(d)

(e)   **(f)**

Figure 12. Ray-traced traveltime shifts for common midpoints located at $x = 1.1$ km (above the reservoir edge, left column) and at $x = 2$ km (outside the reservoir, right column). The reflector depth in a) and b) is 0.85 km (solid lines) and 1.5 km (dashed); in c) and d), the depth is 2 km (solid) and 2.5 km (dashed); and in e) and f), the depth is 2.7 km (solid), 3 km (dashed) and 4 km (dash-dotted).

(a)   **(b)**

(c)

Figure 13. Decomposition of the traveltime shifts computed from approximation (8) for a CMP above the reservoir centre. The shifts caused by the a) isotropic and b) anisotropic velocity changes; c) the total shifts.

weakly dependent on offset (also see Fig. 11c), especially for the reflections from the base of the reservoir.

'homogeneous host rock' models with a relatively rigid reservoir, the reflections from the base of the reservoir and interfaces close to it exhibit the smallest offset variation of the shifts, particularly if the CMP is above the reservoir centre (Fig. 11c). The near-offset traveltime shifts for the deepest reflectors (3 km and 4 km) are close to those for the reflector immediately below the reservoir at a depth of 2.7 km. The offset variation of the shifts in Figs 11(e), 12(e) and 12(f) increases gradually with reflector depth because reflections from deeper interfaces are less influenced by the almost constant velocity perturbations inside the reservoir.

Figure 13 clearly demonstrates that traveltime shifts are caused largely by the deviatoric strains, which also control the offset variation of the shifts for reflectors both above and below the reservoir. Because the deviatoric strains inside the reservoir are almost constant, there is a large spacing between the contours of traveltime shifts beneath the reservoir. This is an indication that the shifts for the deeper reflectors are
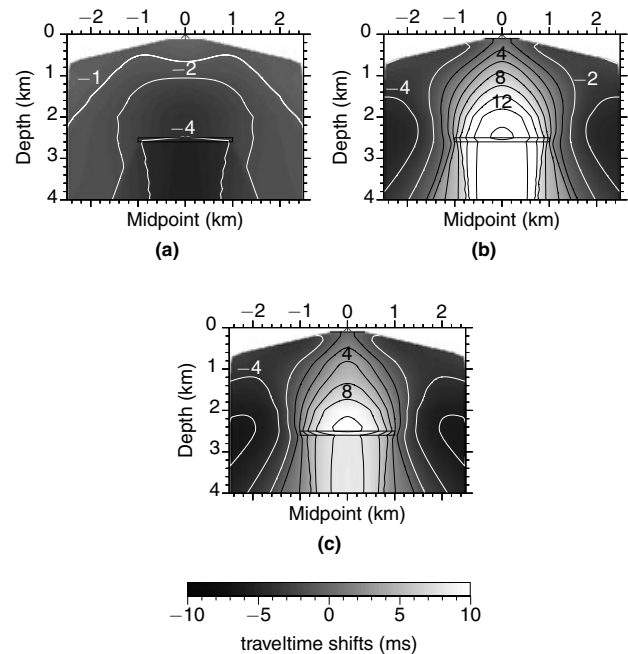
Influence of reservoir shape

The subsurface strain distribution caused by reservoir compaction also depends on the shape of the reservoir (e.g., Faux, Downes and O'Reilly 1997). Because pore-pressure changes inside the reservoir are equilibrated, they cause the reservoir to contract equally in all directions. As a result, one of the principal strain directions should be perpendicular to the reservoir boundaries. For example, the principal in-plane strain directions outside a cylindrical reservoir are parallel to the radius of the reservoir cross-section. Therefore, if the origin of the coordinate system coincides with the reservoir axis, compaction-related shear strains outside the reservoir vanish only along the coordinate axes (Fig. 14a).

For reservoirs with an elliptical cross-section, the shear strains exhibit a similar behaviour but the strain distribution is influenced by the elongation of the ellipse. The largest shear strains move toward the area with the highest curvature of the ellipse (Fig. 14b). As the aspect ratio of the elliptical cross-section decreases, the shear strains tend to accumulate
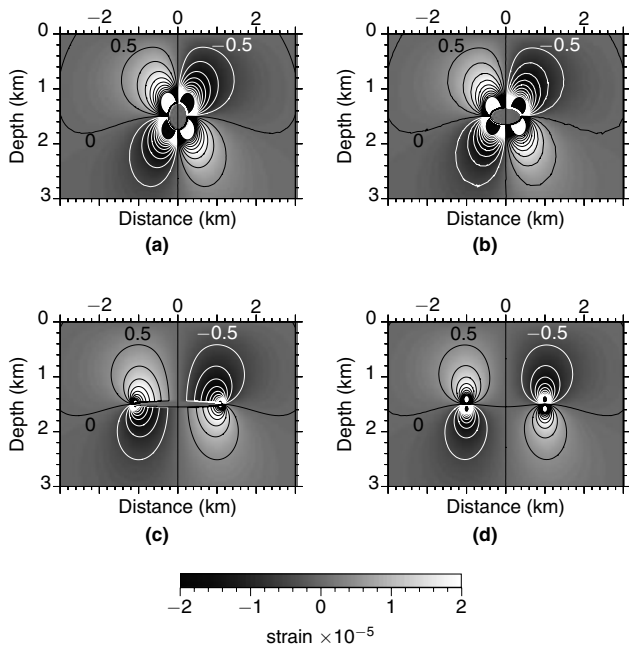
Figure 14. Shear strain $\Delta\varepsilon_{13}$ around compacting reservoirs of different shapes. The reservoir cross-section is a) circular, b) elliptical with the aspect ratio 1/4, c) elliptical with the aspect ratio 1/20 and d) rectangular with the aspect ratio 1/20; the area of the cross-section is fixed. The model parameters are taken from Fig. 1, with no elastic contrast between the reservoir and host rock (i.e., the background is homogeneous).
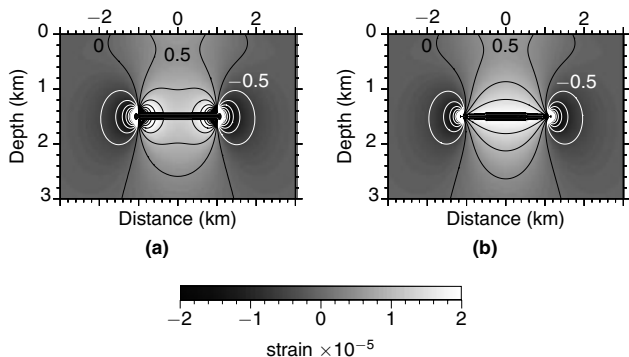

Figure 15. Vertical deviatoric strain $\Delta\varepsilon_{33}$ for reservoirs with a) rectangular and b) elliptical cross-sections. The area of the cross-section and its aspect ratio (1/20) are the same. The model parameters are taken from Fig. 1.

near the reservoir endpoints and the strain distribution resembles that for a rectangular reservoir (compare Figs 14c and 14d).

Figure 15 shows a comparison of the vertical deviatoric strains for rectangular and elliptical reservoirs with the same

area and aspect ratio. The spatial distribution and magnitude of the strains for both reservoir shapes are similar, except for the more pronounced strain accumulation near the vertical edges of the rectangular reservoir. We conclude that the reservoir shape (provided the area and aspect ratio are fixed) does not significantly influence the properties of traveltime shifts, especially for reflectors above the reservoir.

DISCUSSION

Since our analysis is restricted to elastic deformation both inside and outside the reservoir, the modelled traveltime shifts result primarily from the compaction-induced velocity perturbations. Traveltime shifts caused by the geometric changes may become significant, for example, due to the displacement of sources and receivers caused by tides. Such phenomena may have to be taken into account when analysing marine time-lapse data.

We believe that anelastic deformation would not significantly change the behaviour of traveltime shifts above a compacting reservoir. Indeed, Chin and Nagel (2004) showed that the large compaction and subsidence at the Ekofisk field can be explained by restricting anelastic deformation to the reservoir itself. Hence, as long as the anelastic deformation is kept constant throughout the reservoir or inside its compartment, the stress/strain distribution above the reservoir should remain similar to that discussed above. For reflections from interfaces beneath the reservoir, traveltime shifts are still likely to be governed mostly by the anisotropic velocity changes. Indeed, anelastic deformation induces fracturing inside the reservoir, which not only enhances velocity anisotropy but also reduces seismic velocities (Sinha and Plona 2001). This reduction can potentially compensate for the increase in the isotropic velocity perturbations caused by the volumetric contraction of the reservoir.

Compaction-related deformation is treated here as a static problem. In particular, we do not consider coupling between poroelastic deformation and fluid flow inside the reservoir. Although this coupling allows for the pore pressure inside the reservoir to be influenced by the deformation of the host rock and vice-versa (Gutierrez and Lewis 2002), such interaction can likely be ignored over the typical interval between time-lapse seismic surveys (i.e., two years or less). Also, we assumed pore-pressure to be constant (equilibrated) inside the reservoir. If such equilibration does not occur, velocity perturbations may vary spatially inside the reservoir, which may enhance the offset variation of traveltime shifts for reflections from deep interfaces.

Finally, the paper does not address potential problems in accurately measuring traveltime shifts on prestack seismic field data. Such problems range from the repeatability of the acquisition parameters, potentially influenced even by time-lapse temperature variations in the water column (e.g., Landrø and Osdal 2009), to distortions caused by measuring time shifts on partial stacks generated for a certain offset range.

CONCLUSIONS

We studied the influence of heterogeneity of the background model on compaction-related traveltime shifts and their variation with offset. The main goal of the numerical simulations was to verify whether prestack analysis of traveltime shifts provides useful information for reservoir characterization in the presence of background heterogeneity.

When the reservoir is embedded in a medium with different elastic properties, the contrast in the rigidity modulus μ may cause substantial changes in the compaction-related strains. In particular, the contrast in μ influences the relative magnitude of the deviatoric strains responsible for the anisotropic velocity perturbations. Still, the most pronounced isotropic velocity changes (which are related to the volumetric strain) are largely restricted to the reservoir itself. Therefore, as is the case for homogeneous background models, offset-dependent traveltime shifts are mainly governed by the compaction-induced velocity anisotropy. Thus, the offset variation of traveltime shifts estimated from prestack data can provide useful information about the compaction-induced deviatoric strains.

The numerical experiments allowed us to formulate some simple 'rules of thumb' about the properties of the strain field and traveltime shifts. For example, if the reservoir is more rigid than the host rock, the deviatoric strains tend to increase (compared with the homogeneous background model) outside the reservoir and decrease inside it. Hence, the largest offset variation of traveltime shifts for a rigid reservoir is observed for reflectors in the overburden.

The geomechanical modeling for a realistic layered background medium indicates that vertical heterogeneity does not dramatically alter the compaction-induced strain. For example, the magnitude of the deviatoric strains in each layer is inversely proportional to the squared P-wave velocity, while the magnitude of the volumetric strain is also inversely proportional to the squared P-to-S velocity ratio. Moreover, despite the strain discontinuities across layer boundaries, the spatial distribution of strain is generally similar to that for models with a simpler background. In particular, because the reservoir in the layered model is more rigid than the over-

burden, the volumetric strain dominates inside the reservoir, while the deviatoric strains accumulate mostly above it. The deeper layers are stiffer and less strain-sensitive than the rest of the background model, which also contributes to the concentration of the strain-induced velocity perturbations in the upper part of the section. Therefore, the most pronounced offset variation of traveltime shifts is observed for overburden reflections, especially for common midpoints located close to the reservoir edge.

We also showed that reservoirs that have rectangular and elliptical cross-sections with the same area and aspect ratio produce similar spatial distributions of the compaction-induced strains. As a result, the magnitude and offset variation of traveltime shifts are insensitive to such differences in the reservoir shape.

REFERENCES

Červený V. 2001. *Seismic Ray Theory*. Cambridge University Press. ISBN 0521018226.

Chin L.Y. and Nagel N.B. 2004. Modeling of subsidence and reservoir compaction under waterflood operations. *International Journal of Geomechanics* **4**, 28–34.

Downes J.R., Faux D.A. and O'Reilly E.P. 1997. A simple method for calculating strain distributions in quantum dot structures. *Journal of Applied Physics* **81**, 6700–6702.

Faux D.A., Downes J.R. and O'Reilly E.P. 1997. Analytic solutions for strains distributions in quantum-wire structures. *Journal of Applied Physics* **82**, 3754–3762.

Fuck R.F., Bakulin A. and Tsvankin I. 2009. Theory of traveltime shifts around compacting reservoirs: 3D solutions for heterogeneous anisotropic media. *Geophysics* **74**, D25–D36.

Fuck R.F. and Tsvankin I. 2009. Analysis of the symmetry of a stressed medium using nonlinear elasticity. *Geophysics* **74**, WB79–WB87.

Guilbot J. and Smith B. 2002. 4D constrained depth conversion for reservoir compaction estimation: Application to Ekofisk field. *The Leading Edge* **21**, 302–308.

Gutierrez M.S. and Lewis R.W. 2002. Coupling of fluid flow and deformation in underground formations. *Journal of Engineering Mechanics* **128**, 779–787.

Hatchell D.P.J. and Bourne S.J. 2005a. Measuring reservoir

compaction using time-lapse time shifts. 75th SEG meeting, Houston, Texas, USA, Expanded Abstracts, 2500–2503.

Hatchell P. and Bourne S. 2005b. Rocks under strain: strain-induced time-lapse time-shifts are observed for depleting reservoirs. *The Leading Edge* **24**, 1222–1225.

Herwanger J. and Horne S. 2005. Predicting time-lapse stress effects in seismic data. *The Leading Edge* **24**, 1234–1242.

Herwanger J.V. and Horne S.A. 2009. Linking reservoir geomechanics and time-lapse seismics: Predicting anisotropic velocity changes and seismic attributes. *Geophysics* **74**, W13–W33.

Hodgson N., MacBeth C., Duranti L., Rickett J. and Nihei K. 2007. Inverting for reservoir pressure change using time-lapse time strain: application to Genesis field, Gulf of Mexico. *The Leading Edge* **26**, 649–652.

Hu S.M. 1989. Stress from a parallelepipedic thermal inclusion in a semispace. *Journal of Applied Physics* **66**, 2741–2743.

Landrø M. and Osdal B. 2009. Estimation of water column velocity and thickness changes from 4D seabed diffraction analysis. 71st EAGE meeting, Amsterdam, the Netherlands, Expanded Abstracts, V023.

Landrø M. and Stammeijer J. 2004. Quantitative estimation of compaction and velocity changes using 4D impedance and traveltime changes. *Geophysics* **69**, 949–957.

Press W.H., Teukolsky S.A., Vellerling W.T. and Flannery B.P. 1992. *Numerical Recipes in C – The Art of Scientific Computing*, 2nd edn. Cambridge University Press. ISBN 818561816X.

Prioul R., Bakulin A. and Bakulin V. 2004. Nonlinear rock physics model for estimation of 3D subsurface stress in anisotropic formations: theory and laboratory verification. *Geophysics* **69**, 415–425.

Røste T., Stovas A. and Landrø M. 2006. Estimation of layer thickness and velocity changes using 4D prestack seismic data. *Geophysics* **71**, S219–S234.

Sarkar D., Bakulin A. and Kranz R.L. 2003. Anisotropic inversion of seismic data for stressed media: theory and a physical modeling study on Berea sandstone. *Geophysics* **68**, 690–704.

Segall P. 1992. Induced stresses due to fluid extraction from axisymmetric reservoirs. *Pure and Applied Geophysics* **139**, 535–560.

Segall P., Grasso J.R. and Mossop A. 1994. Poroelastic stressing and induced seismicity near the lacq gas field, southwestern France. *Journal of Geophysical Research* **99**, 15,423–15,438.

Sinha B.K. and Plona T.J. 2001. Wave propagation in rocks with elastic-plastic deformations. *Geophysics* **66**, 772–785.

Soltanzadeh H., Hawkes C.D. and Sharma J.S. 2007. Poroelastic model for production- and injection-induced stresses in reservoirs with elastic properties different from the surrounding rock. *International Journal of Geomechanics* **7**, 353–361.

Sylte J.E., Thomas L.K., Rhett D.W., Bruning D.D. and Nagel N.B. 1999. Water induced compaction in the Ekofisk field. SPE meeting, Houston, Texas, USA, Expanded Abstracts, 56426.

Wang H.F. 2000. *Theory of Linear Poroelasticity with Applications to Geomechanics and Hydrogeology*. Princeton University Press. ISBN 0691037469.

Yale D.P. and Jamieson Jr. W.H. 1994. Static and dynamic mechanical properties of carbonates. In: *Rock Mechanics Models and Measurements Challenges from Industry. Proceedings of the 1st North American Rock Mechanics Symposium* (eds P.P. Nelson and S.E. Laubach), pp. 463–471. Balkema. ISBN 9054103858.